Calibration of Gantry-Tau Robot and Prototyping of Extruder for 3D Printing

Patrik Lilja

Jorge Sola Merino

LUND UNIVERSITY

Department of Automatic Control

MSc Thesis
ISRN LUTFD2/TFRT--5978--SE
ISSN 0280-5316

Department of Automatic Control
Lund University
Box 118
SE-221 00 LUND
Sweden

Printed in Sweden by Tryckeriet i E-huset
Lund 2015

Abstract

This master thesis is about improving the accuracy of a Gantry-Tau robot by identifying the key parameters in the kinematics of the robot. This is done using a vision system and then estimating the parameters by minimizing the closure equation of the kinematics. The robot with improved control is then used for additive manufacturing. Furthermore, a prototype for a large plastic printer head is presented.

Acknowledgements

First of all, we would like to thank our supervisors Anders Robertsson and Martin Holmstrand for their constant support throughout the thesis, their suggestions, and their patience. We would also like to thank Björn Olofsson for his support when we dealt with problems regarding the camera measurement system. Borja Serra also deserves our thank, due to the mutual motivation and suggestions that we gave each other. And finally, thanks to Sonia Guijarro for her feedback, and Rolf Johansson for giving us his valuable opinion and being our examiner.

Contents

1

Introduction

1.1 Background

3D printing or additive manufacturing (AM) is a process where a three dimensional object is constructed by laying down layers of material under computer control. This can be accomplished in a variety of different procedures. The technology is not new, as it was developed in the 1980s. In 2005 inexpensive printers were made affordable to the public through the RepRap and Fab@Home projects [*RepRap Project* 2015][*Fab@Home Project* 2015]. The RepRap project successfully developed a 3D printer that can print most of its own parts, targeted towards private customers and small businesses.

As technology progresses and 3D printers are becoming more and more affordable it might lead to a change in consuming patterns. Instead of buying factory-made simple plastic details, in the future the customer could print it on demand, on site. In 2014 NASA sent the first item, a ratchet wrench, via e-mail to the International Space Station to be printed in space [NASA, 2014].

Although 3D printing in the industry is still limited, there have been extensive efforts to expand into this new way of manufacturing worldwide. Promising future application areas are aerospace, automotive and electronic industries [Zhang et al., 2014]. This makes 3D printing an interesting industry that is predicted to be worth $12.8 billion by 2018 [*Wohlers Associates* 2014].

What makes this technology very interesting to industry is the fact that it is able to create extremely complicated shapes that conventional subtractive manufacturing processes would not be able to replicate. For example AM can be used to print moving parts such as cogwheels already assembled. Another aspect is that there is almost no waste of material, since AM only uses the material that it needs to make the part, except for support material whereas in traditional subtractive manufacturing processes, such as CNC milling, almost 95% of the raw material is often wasted [Excell and Nathan, 2010].

In Table 1.1 a rough timeline for the uses of AM is shown. It can be seen that we are currently in a period where the size of the objects manufactured are both shrinking and growing. For the applications where the printed object is growing, in-

1988-1994	Rapid prototyping
1994	Rapid casting
1995	Rapid tooling
2001	AM for automotive
2004	Aerospace
2005	Medical (polymer jigs and guides)
2009	Medical implants (metals)
2011	Aerospace (metals)
2013-2016	Nano-manufacturing
2013-2017	Architecture
2013-2018	Biomedical implants
2013-2022	In situ bio-manufacturing
2013-2032	Full body organs

Table 1.1 The timeline for AM applications [Zhang et al., 2014].

dustrial robots are an alternative for moving the printer head that is both flexible and cost effective. The concept of using an industrial robot for 3D printing is similar to using an industrial robot with a cutting spindle, to replace some applications of an expensive CNC machine. Currently most industrial robots used for 3D printing are serial robots. But it has been determined that for some applications parallel kinematic robots are preferable due to the inherent properties of the parallel structure [Zhang et al., 2014].

2

Problem formulation

2.1 Goals

The goal of this thesis is to calibrate and control a parallel kinematic robot for 3D printing using either concrete or plastic. For this purpose, the L2 and F1 Gantry-Tau robots at Lunds Tekniska Högskola (LTH) are to be used in this thesis.

Another objective is to print with a reasonable speed and as high accuracy as possible. Since there exists no commercial printer head for printing large volumes of plastic suitable for large industrial robots it is decided that a custom printer head should be designed. The design goal for the printer head is to have a large output flow to print large parts in a relatively short time. To achieve this an extrusion design with fused deposition modeling is chosen. The design is inspired by an existing printer head developed by the Dutch designer Dirk van der Kooij [Halterman, 2013].

2.2 Demarcation

Due to time limitations the scope of the thesis has been reduced. The L2 robot was out of service for some time and that was a setback for the project, as the verification of the optimization was delayed. Hence the initial plans to calibrate and print using the F1 robot had to be canceled. Furthermore the goal of developing a plastic printer head was added very late in the process and should be seen as a starting point for future work. A theoretical design was made and the prototype was finished but not fully tested.

2.3 Outline

In Chapter 3 the theory and the structure of the robots and how to control them will be explained briefly. The basic theory of plastic extrusion is also covered. Chapter 4 will explain how the experiments done in the thesis are conducted and also how the plastic extruder is designed. The results are then presented in Chapter 5. The conclusions of the results are stated in Chapter 6 and then possible future work is discussed in Chapter 7.

3

Theory

3.1 Gantry-Tau robots

In this section the L2 and F1 robots are introduced. The L2 and F1 robots were created by ABB and Güdel AG in collaboration with Lund University for research purposes within the EU-Fp6/Fp7 projects SMErobot and ECHORD/MONROE [SMErobot, 2015][MONROE, 2015]. Both are located at LTH. Both robots are parallel kinematic manipulators (PKM) with a 3-2-1 setup, called Gantry-Tau robots. A picture of the structure can be seen below in Figure 3.1. Pictures of the L2 robot and the F1 robot are shown in Figure 3.2 and Figure 3.3.

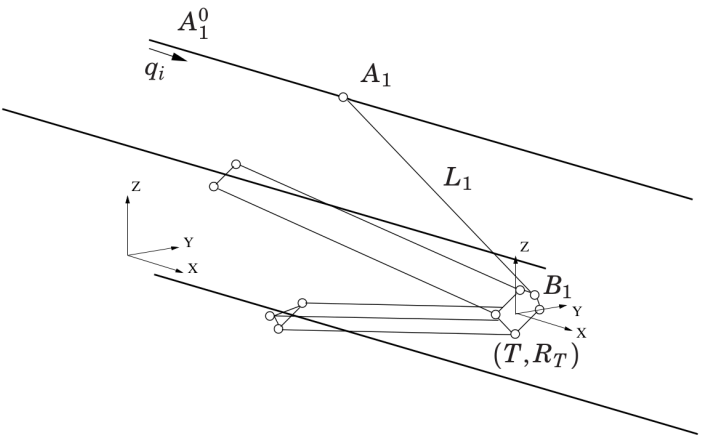

Figure 3.1 Structure schematic of a Gantry-Tau robot. Denotations are shown for arm 1. Explanations of parameters and variables are found in Table 3.1 [Dressler, 2012].

Figure 3.2 The L2 robot located in the Robot Lab at LTH.

A_i^0	Home position of the cart ($q_i = 0$)
q_i	Position of cart on rail
A_i	Arm i connection to cart
B_i	Arm i connection to end-effector plate
L_i	Length of arm i
T	Tool position
R_T	Tool orientation

Table 3.1 Explanation of variables and parameters, see Figure 3.1.

The Gantry-Tau robot consists of three parallel rails on which three carts can move independently. To these carts arms are attached. Each arm consists of a cluster of links. Arm 1 has one link, arm 2 has two links and arm 3 has three links. Hence this is called a 3-2-1 setup. The links on arm 2 and arm 3 form parallelograms. This configuration, in the nominal case, ensures that the end-effector plate maintains a constant rotational orientation when the carts move. This makes all movement in the ideal case purely translational.

An advantage over conventional serial robots is that the parallel setup provides a lower weight of the moving part of the robot. This results in a lower inertia, allowing for greater acceleration. The parallel setup also makes the robot stiffer. These properties gives the robot large accuracy and repeatability. Another advantage is that the workspace can be made arbitrarily large in the direction of the rails by extending the length of the rails. A drawback is reduced orientation of the end-effector and

Figure 3.3 The F1 robot located at Ingvar Kamprad Designcentrum at LTH. [Dressler, 2012].

thus a restriction in viable tasks.

To achieve more degrees of freedom more motors can be added. For the robots used in this thesis this has been done in different manners. The L2 robot has 5 degrees of freedom (DOF). The first three are achieved as described above, and then two rotational actuators have been added to a wrist to give 5-DOF, as seen in Figure 3.2. This means that there is no means of adjusting the pitch of the end-effector.

The F1 robot has 6-DOF. To get the last tree degrees of freedom and thus achiev-

ing reorientation within 15° - 30° depending on rotation axis [Dressler, 2012], one more motor is added to cart 2 and two to cart 3. The motor on cart 2 can rotate the links, same as the first on cart 3. The second motor on cart 3 can tilt the platform that the links are attached to. Another property of the F1 robot is that it is operates vertically whereas the main motion of L2 is in the horizontal direction.

3.2 Kinematics

Robot kinematics are traditionally divided into two problems. The first is to find the location T and orientation R_T of the end-effector as a function of the states of the actuators q, and possibly a configuration set c if more than one solution exists. As an extra set of variables one might also include kinematic parameters s, i.e., the non nominal lengths of the links or arms of the robot. This is called the forward kinematics:

$$[T, R_T] = f_{fk}(q, s, c) \tag{3.1}$$

The second problem is to know the state of the actuators given the location and orientation of the end-effector, i.e., the inverse kinematics. This is also dependent on kinematic parameters and possibly additional configuration options:

$$q = f_{ik}(T, R_T, s, c) \tag{3.2}$$

Contrary to traditional serial robots the inverse kinematics are easier to solve than forward kinematics for a PKM [Dressler, 2012].

3.2.1 Kinematics for the 3-DOF Gantry-Tau robot

For the nominal case a simplified model of the geometry can be used, see Figure 3.4. This is due to the constant orientation of the end-effector owing to the Gantry-Tau configuration.

The two coordinate frames shown are the world frame and the end-effector frame. The number of links in each arm in this model has been reduced to one. v_i is the direction vector of the rails, here in the nominal case identical for all three rails. A_1,A_2 and A_3 can then be expressed as

$$A_i = A_i^0 + q_i \cdot v_i. \tag{3.3}$$

The kinematic constraint of these arms can now be independently expressed as

$$L_i = \| A_i^0 + q_i \cdot v - T \| . \tag{3.4}$$

From this constraint q_i can easily be calculated independently for the inverse kinematics.

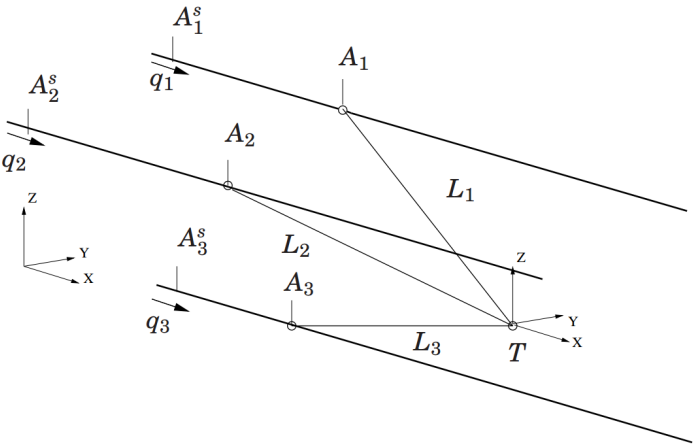

Figure 3.4 Simplified schematic of a Gantry-Tau robot. Explanations of parameters and variables are found in Table 3.1 [Dressler, 2012].

To solve the forward kinematics, i.e., solving (3.4) for T for the three arms, is equivalent to solving the intersection of three spheres, see Figure 3.5. This problem is know as trilateration.

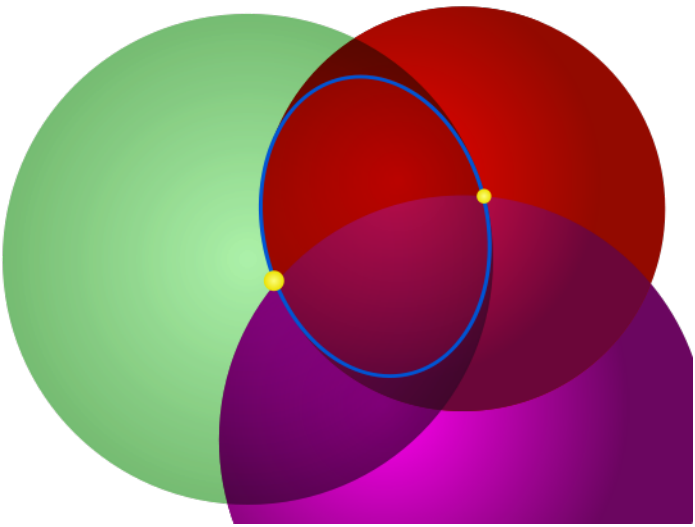

Figure 3.5 The intersection of three spheres has two solutions as seen above. [*Wikipedia. Triangulering*]

This is a well known problem that can be solved by e.g., Gaussian elimination or orthogonal decomposition [Coope, 2000].

3.2.2 Kinematics for the 6-DOF Gantry-Tau robot

As previously mentioned the F1 robot has three additional motors to achieve 6-DOF as shown in Figure 3.6. If the rotation of the plates of cart 2 and 3 are controlled so that $q_4 = -q_5$, the end-effector position and orientation can be decoupled and considered independently. Then an analytical solution exists, but the degrees of freedom have been reduced to five, as the end-effector cannot rotate around the X-axis. When this constraint is fulfilled the links will always form parallelograms.

For the 6-DOF forward and inverse kinematics, iterative numerical methods must be used e.g., Newton-Raphson. This is explained in detail in [Dressler, 2012].

F1 also has one extra motor on each cart to minimize backlash, giving a total of nine motors [Robertz et al., 2010].

3.3 3D printer head

A design concept for a 3D printer head for plastic output is presented in this section. The design of a 3D printing head is analogous to the one of an extruder for plastic injection moulding, except for the fact that the plastic extruder is designed for a continuous process.

The criteria for the design of the plastic extruder has been to maximize the output flow in order to print large parts within a relatively short period of time and thus, taking advantage of the potential of industrial robots like the ones studied in this thesis.

3.3.1 Extruder generalities

An extruder is a machine designed to force a material through a die. There are different ways to perform this task such as single screw extrusion, or twin screw extrusion. However this design is focused on the single screw extrusion [*Wikipedia. Plastic extrusion*].

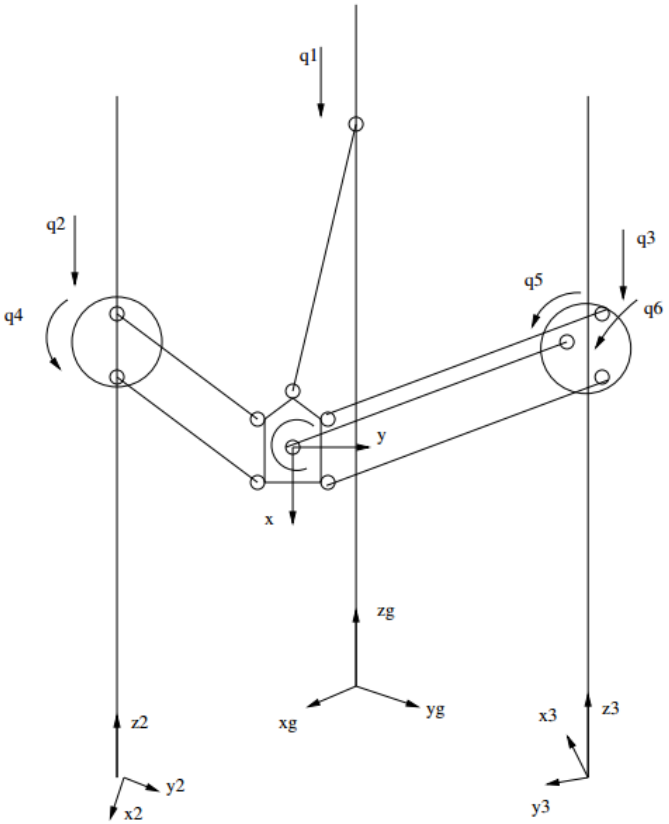

Figure 3.6 A schematic model of the F1 robot [Dressler, 2012].

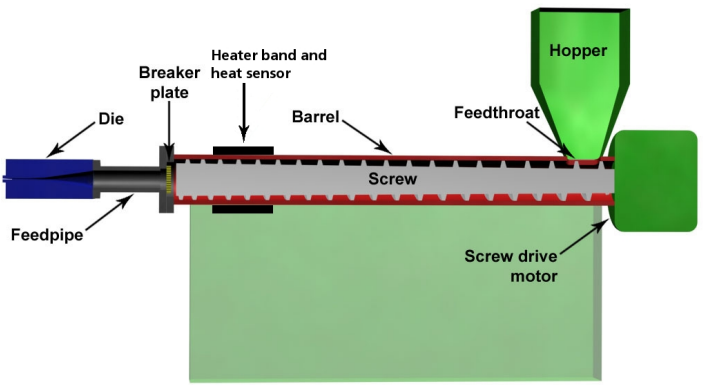

Figure 3.7 Schematics of a generic single screw extruder. [*Wikipedia. Plastic extrusion*]

A single screw extruder may include the components listed and explained in the following subsection.

3.3.2 Components of an extruder

- **Die:** The die is the hole which the material to be extruded is pressed through. The shape of the die determines the shape of the cross section of the extruded material. In this project a nozzle with a circular section works as the die.

- **Screw:** The screw is used to transport the extrusion material through the barrel and push it against the die. One of the reasons that the material are partially heated is because of the friction and high pressure produced during this procedure.

  The screw is one of the most important parts of the extruder and it is defined mainly by its diameter and its length. There are other parameters that define the geometry of the screw such as pitch, helix angle etc. as shown in Figure 3.8. These parameters are not considered in this design.

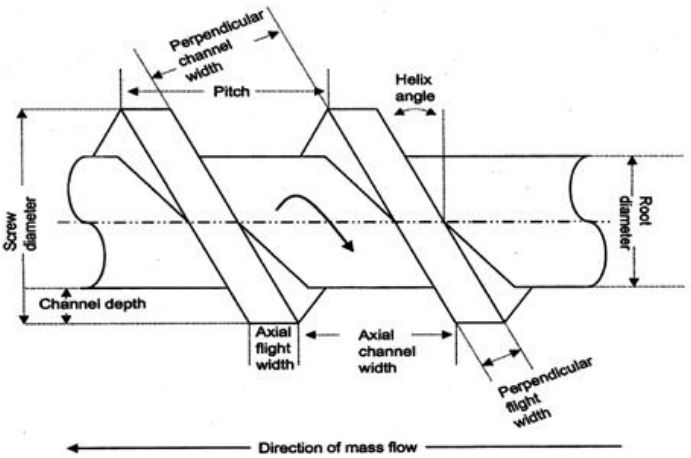

Figure 3.8 Schematics of a generic extrusion screw. [*SolidsWiki. Extrusion Screws*]

The diameter, D, of the screw is the most important parameter since the rest of the extruder is designed using this parameter as a starting point. This parameter has a large effect on the overall performance of the extruder, mainly the final output flow and needed torque, as will be explained in the next section.

The length, L, which is usually expressed as a number multiplied by the diameter of the screw. A higher length implies a bigger extruder, with a better mixing of the plastic and less sensitive to changes of pressure in the die [H. F. Giles and Mount, 2005].

- **Barrel:** The barrel is a metallic tube that wraps the screw. It has to fit the screw in the right way to avoid leakages. It has to withstand mechanical stress and the temperature from the melting process.
- **Hopper:** The extruder is fed with pellets, i.e., plastic balls, and the hopper must be designed to continuously feed the extruder and be thermally insulated to avoid premature melting of the plastic.
- **Heating and cooling element:** Usually the heating element consists of heating bands encircling the barrel coupled with temperature sensors and a temperature control unit to keep a stable and gradually increasing temperature of the plastic. Several heating units might be added to achieve higher precision temperature control. The excess heat is dissipated by passive air cooling in most cases.
- **Driving unit:** it usually consists of an electrical motor and usually a gearbox to adapt the motor performance to the needs of the extruder, i.e., high torque and low speed. The driving unit is supposed to drive the screw with a constant speed, thus a control system is usually designed for this task.

3.3.3 Quantitative model of the extruding process

The extruding process is a complex problem that combines different disciplines such as fluid dynamics, thermodynamics, material science, etc. A large number of parameters has to be taken into consideration. This makes for a very complicated model of the process. Therefore a quantitative approach is used in this thesis. In [Manias, 2012] a quantitative analysis of the output flow of the extruder is done. The analysis concludes after some simplifications in the following model:

$$Q \propto N \cdot D^3 \tag{3.5}$$

So the volumetric flow Q is proportional to the speed N of the screw and grows with the cube of the diameter D.

In reference [Medeni Maskan, 2011], it is also explained that the needed torque scales up in a similar way for similar materials and shape of the extruder.

$$T \propto L \cdot D^3 \tag{3.6}$$

As it can be seen, the torque T also scales with the cube of the diameter, and linearly with the length L.

3.3.3.1 Extruder and die characteristics model In [A. W. Birley and Batchelor, 1992] a more complex model is explained, where the die works as a flow restriction. This creates a pressure gradient, ΔP, along the extruder that works against the flow. Thus the net volumetric flow could be expressed as the drag flow, Q_d, produced by the screw movement plus the pressure flow, Q_p:

$$Q_e = Q_d + Q_p \tag{3.7}$$

$$Q_d = \alpha N \tag{3.8}$$

$$Q_p = -\frac{\beta}{\mu}\Delta P \tag{3.9}$$

where α and β are geometric parameters of the screw and μ is the fluid viscosity. The drag flow depends linearly on the speed, as explained in the previous model. The relation between the pressure drop and the flow in the die for a circular section is defined by:

$$Q_n = \frac{\pi R_d^4 \Delta P}{8 L_d \mu} \tag{3.10}$$

where R_d and L_d are the radius and the length of the die. For a given speed, die geometry and screw geometry, the net flow would be given by solving the equation system formed by (3.7) and (3.10). In the operating point of the extruder $Q_e = Q_n = Q$. In the case where there is no flow restriction (open discharge), $Q = Q_d$ and $Q_p = 0$, and in closed discharge $Q = 0$ and $Q_d = -Q_p$.

The extruder and die characteristics model is an useful model to understand the way extruders work and to estimate values for an initial prototype. Nevertheless it is important to highlight that despite being a more complex model, it still assumes some simplifications such as considering the fluid as Newtonian, and assuming that all the pressure drop will happen in the die.

3.3.3.2 Lyman Filament Extruder Designed by Hugh Lyman, it is one of the first available open source extruders. Since it was released its design has been developed with new versions, and it is the best documented extruder project. In Table 3.2 some of the important parameters are shown. All of them are extracted from the available documentation about the project, and thus some result might not be well justified, but serve as a good estimation and reference starting point [Lyman, 2012].

Holding torque (Nm)	2.942
Speed (rpm)	13.5
Output flow (kg/h)	0.125
Diameter of screw (mm)	16
Length of screw (mm)	142

Table 3.2 Parameters of Lyman filament extruder.

These values will be used in Section 4.4.2 for scaling up the design and determine new parameters for this project.

4

Method

4.1 Equipment

In order to perform calibrations for the L2 robot a vision system made by Nikon is used. This vision system includes the so called K600 cameras which track infrared light emitted by IR LEDs, see Figure 4.1. This is done with high single point accuracy, up to 60μm [*K-Series Optical CMM solutions* 2010]. This technique is also called DMM, which stands for Dynamic Measuring Machine. Other essential components of the DMM system are the DMM software, the LED strobe units, infrared LEDs and the SpaceProbe which is used to define geometries.

To perform experiments and read data from the robot and camera the Nikon DMM software is used together with ExtCtrl software and custom DMM software. The ExtCtrl software allows for low-level access to i.e., motor angles and sensor signals. Using a Simulink model that compiles to real time code it is then possible to alter these signal before forwarding them to the robot [Blomdell et al., 2010]. Using the forward and inverse kinematics mentioned in Section 3.2 it is possible to make changes to the Cartesian coordinates.

Both the custom DMM software and ExtCtrl software have been developed at the Robotics lab, LTH. The DMM software was chiefly made by Björn Olofsson, though GUI was made by Anders Blomdell.

4.2 Calibration

The aim is to determine the optimal kinematic parameters of the L2 robot. These parameters are the arm lengths, the direction vectors for the rails assuming no parallelism, and the home position vector for the ball joints. For this measurement the DMM system described in Section 4.1 is used. As a first step, a measurement frame is created with the help of the SpaceProbe, see Figure 4.2. This frame has its X axis pointing in the direction of the rails, the Z axis against gravity, forming a right-handed coordinate system. LEDs are placed on the motors of the carts as shown in Figure 4.3 and also on the end-effector as shown in Figure 4.4. Since

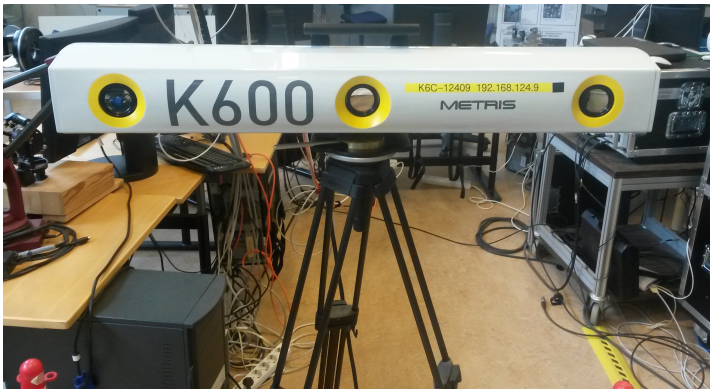

Figure 4.1 Nikon K600 camera used for accurate position measurements.

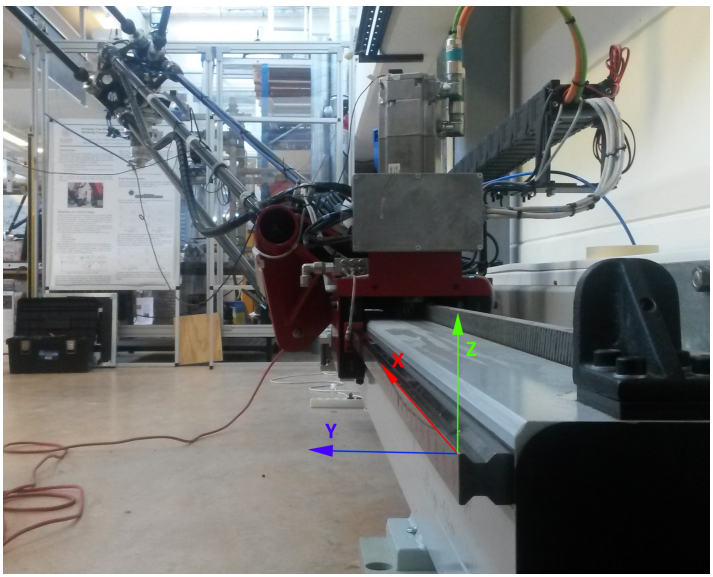

Figure 4.2 The coordinate system defined with the SpaceProbe.

only one LED is placed on the end-effector plate, only position can be measured and not the orientation. If two more LEDs are added, the orientation could also be measured. Measuring the orientation could be part of future work.

The direction vectors of each rail are measured by performing a least squares fit approximation of all the points along the path followed by the carts. The cost

function minimized for each rail is:

$$V = \sum_{i=1}^{n} \left[(x_i, y_i, z_i) - \left((x_0, y_0, z_0) + k_i \cdot (v_x, v_y, v_z) \right) \right]^2 \tag{4.1}$$

where x_i, y_i and z_i are the measured points. The initial position of the motor is denoted (x_0, y_0, z_0), and (v_x, v_y, v_z) are the sought direction vectors that are optimized. The optimization has a constraint that the length of the direction vectors should be one. k_i is defined as:

$$k_i = \sqrt{(x_i - x_0)^2 + (y_i - y_0)^2 + (z_i - z_0)^2} \tag{4.2}$$

Given a set of n joint positions q_i and end-effector poses $T_{m,i}$, and the previously calculated direction vectors, the rest of the kinematic parameters can be identified by minimizing the kinematic constraint (3.4) for each arm. This can be done independently for each arm. The equation to minimize is then:

$$V = \sum_{i=1}^{n} (\| A^0 + q_i \cdot v - T_{m,i} \| - L)^2. \tag{4.3}$$

The optimized parameters are the length L and the ball joint position A^0 when the motors are at home position. In Figure 4.5 a block diagram of the process variables is shown. M is the transfer function between reference position and actual position for the joints, Fk is the ideal forward kinematic function, C is the camera model which represents drifts in the measurements, noise and filtering of the signal and is assumed to be perfect, and d represents disturbances such as backlash, deformations and dynamic effects.

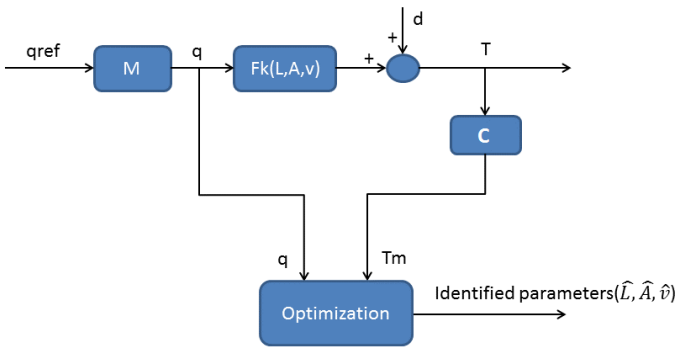

Figure 4.5 Block diagram of the calibration process.

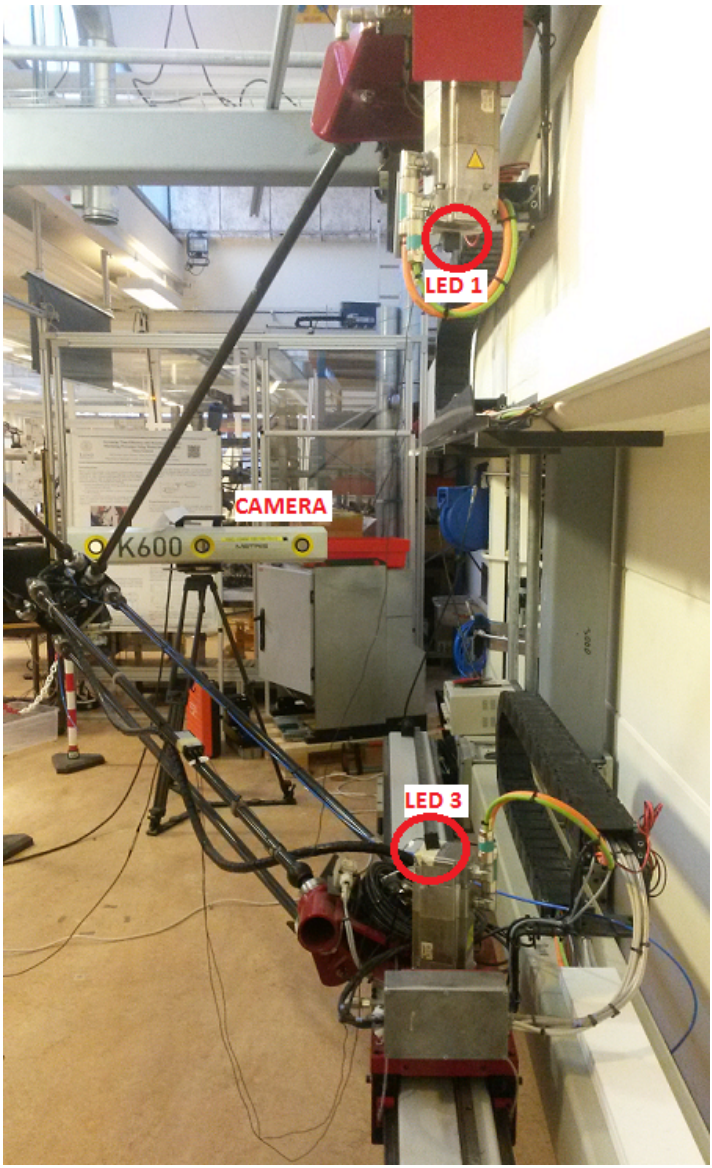

Figure 4.3 Camera and LEDs setup for L2 robot.

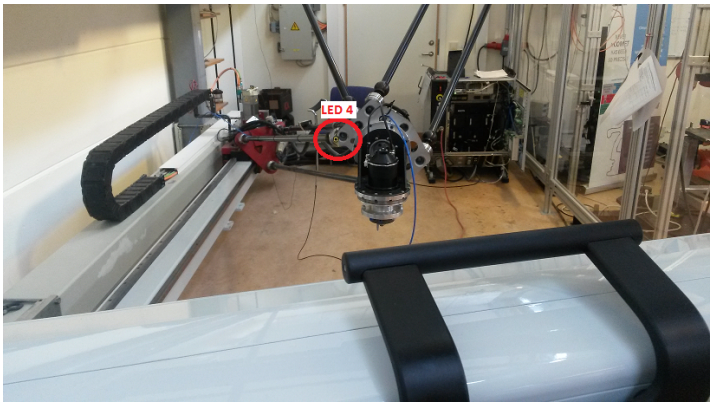

Figure 4.4 Camera and LEDs setup for L2 robot.

For this purpose a RAPID[1] program is created to move the robot in a certain pattern. The pattern is shown in Figure 4.6. The joint positions and measured end-effector positions are recorded with a sample period of 4.032 milliseconds. It is important to highlight that due to camera measurement space limitations, the optimization process is done in a small portion of the workspace and thus the identified parameters might not be the ones that are optimal for the whole workspace [Tyapin et al., 2007].

[1] ABB robots are programed using the RAPID programming language

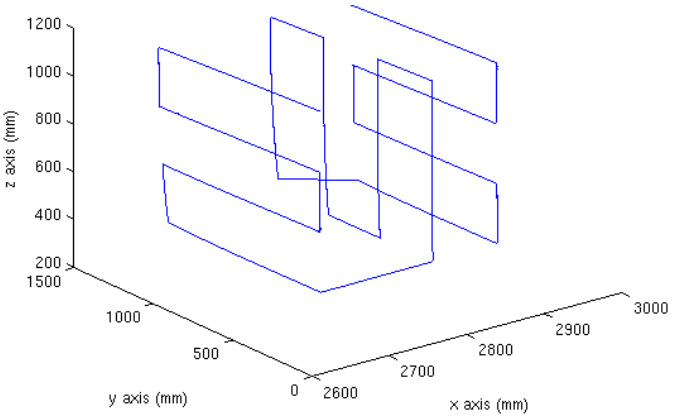

Figure 4.6 The path taken by the end-effector when capturing the position.

4.3 Validation of estimated parameters

Validation of the estimated parameters can be made in both qualitative and quantitative ways. In Chapter 5 both the old kinematic parameters and the newly estimated are presented in Tables 5.1 and 5.2 respectively. The goal is to have a smaller spatial error. A quantitative way to measure this error would be to perform the forward kinematics for a given position of the joints, and compare the output with the one provided by the camera measurement system. A qualitative way would be to perform a certain movement following a pattern and calculate how similar the path followed by the robot is to the ideal path.

4.3.1 Circle experiment

In order to qualitatively evaluate the accuracy of the model an experiment where the robot follows a circle of radius $r = 100mm$ is performed. With all the data points collected a least squares approximation is performed to find the center of the circle that best fits all the points within a plane. The residual error from fitting the circle into the plane can be viewed as a qualitative way of evaluating the new set of parameters. The expressions minimized in the least squares approximation are:

$$\sum_{i=1}^{n}(ax_i + by_i + cz_i + d)^2 \tag{4.4}$$

$$\sum_{i=1}^{n} \left(\sqrt{(x_i - x_0)^2 + (y_i - y_0)^2 + (z_i - z_0)^2} - r \right)^2 \tag{4.5}$$

Here (x_i, y_i, z_i) are the measured points, a, b, c and d are the unknown parameters of the plane and (x_0, y_0, z_0) is the unknown circle center point. Expression (4.4) is first used to obtain the plane that best contains the set of points. In the second optimization using Expression (4.5), which is derived from the equation of a sphere, the estimated plane is used as a constraint when fitting the points.

Since the performance of the robot for a certain set of parameters depends on where in the workspace the end-effector is located, this experiment is performed in four different positions, as shown in Figure 5.6.

4.3.2 Quantitative validation

Another way of validating the accuracy of the model is to measure the difference between a measured end-effector position and a calculated end-effector position. The measured end-effector, $T_{m,k}$, is given using external measurement equipment in the measurement frame. The calculated end-effector is given using forward kinematics, $f_{fk}(q_k, s)$, expressed in the robot frame.

The error is calculated as:

$$e_k = \| \, T_{m,k} - f_{fk}(q_k, s) \, \| \tag{4.6}$$

For this equation to be valid the measured end-effector and calculated end-effector must be expressed in the same frame. To express the measured end-effector in the robot frame it is necessary to find a transformation between the measurement frame and the robot frame.

This could be achieved by using least squares to approximate a transformation matrix. Taking n points in the measurement frame and pairing them with the corresponding points calculated by the forward kinematics in the robot frame, one can under the assumption that they are the same point in space, find a transformation from one frame to the other.

However, this method hides the spatial error caused by the imperfection of the kinematic model, since it assumes that the pair of points are the same, and thus this is not a feasible method to compare different sets of parameters.

Instead of trying to find a transformation in between the robot and the measurement frame, the parameters estimated with the minimization of (4.3), which are expressed in the measurement frame, are used to redefine a new robot frame with the same position and orientation than the measurement frame. This is possible since the orientation of the robot frame does not affect the forward kinematics as long as all the kinematic parameters are referred to that frame.

Once the robot frame is redefined to be equal to the measurement frame, it is possible to compare the estimated values as previously explained. For this experiment measurements in a grid of 48 points are taken. In Figure 4.7 a block diagram

of the validation process is shown. Fk represents the ideal kinematic model, $\widehat{Fk}$ is the identified kinematic model, q is the position of the robot joint, d represents some disturbances, T_m is the measured end-effector position and $\hat{T}$ is the calculated end-effector position.

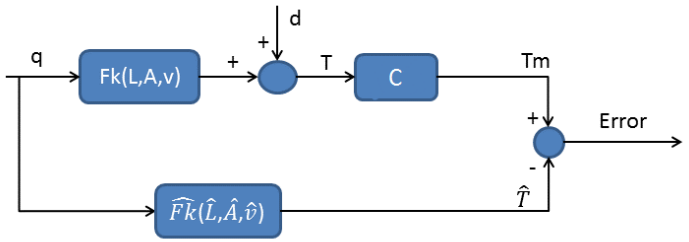

Figure 4.7 Block diagram of the validation process.

4.3.3 Compensation of the systematic error

Once the validation process is done, it is shown in Chapter 5 that there is a systematic error in the three axes that can be compensated. This systematic error might be caused by an inaccuracy in the kinematic model, or in the identified kinematic parameters.

Assuming that the desired position of the end-effector is T_{ref}, by performing the inverse kinematic function the needed joint positions are calculated. However, due to the systematic error in the model, the resulting position measured with the camera T_m differs. In order to compensate for this, the calculated error for each point and each axis is interpolated and extrapolated with the help of a look-up table. The error is then subtracted to the desired three dimensional position, so that this error is compensated and thus, the accuracy is improved.

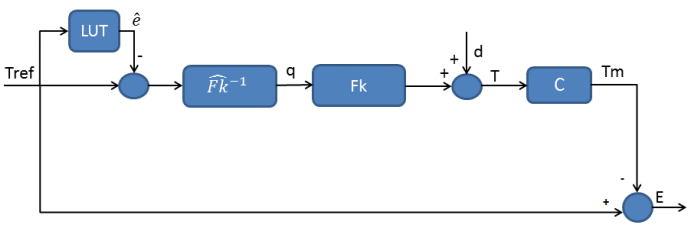

Figure 4.8 Block diagram with compensation of the error.

In figure 4.8, a block diagram shows how the error is compensated for. The block

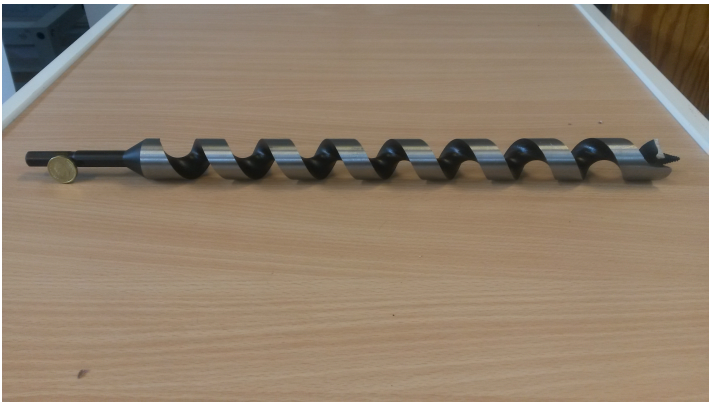

Figure 4.9 Drill bit used as extrusion screw.

LUT represents the look-up table, $\hat{e}$ represents the interpolated or extrapolated error, $\widehat{Fk}^{-1}$ is the inverse of the kinematic model with the identified parameters and E is the spatial error.

4.4 Design of the extruder

As explained in Chapter 3, the design of an extruder is a complex problem and thus, for this design it is decided to start with a few fixed parameters and develop the design according to those parameters.

4.4.1 Screw

Since the screw is one of the most important parts in the extruder, the diameter and geometry of the screw are chosen as the starting point for the design process.

Screws used in extrusion have a complex geometry and use steel alloys making them an expensive part. Instead, a wood drill bit is decided to be used since it has a similar shape (Figure 4.9). It is also made of sturdy material and has enough room for the pellets. Since the goal of the project is to achieve as much flow as possible, the chosen diameter is one of the largest available, 30*mm*, with a length of 460*mm*. The use of drill bits in extruders is not something new and has been documented and its viability is ensured in other open source projects such as the Lyman filament extruder [Lyman, 2012].

4.4.2 Output flow and torque estimation

One of the most important and interesting variables in the extruding process is the output flow that will determine the speed of the printing process. Although the extruder and die characteristics model is an interesting and useful model to describe

the process, a more accurate way to estimate the flow would be using the empirical relations described in Subsection 3.3.3, which are used to scale up parameters and results obtained in the Lyman extruder. According to that, and assuming an aimed output flow of 3kg/h as a starting specification, the following design parameters are obtained:

$$Q_2 = Q_1 \cdot \frac{N_2}{N_1} \cdot \frac{D_2^3}{D_1^3} \tag{4.7}$$

After reordering the equation the result is:

$$N_2 = \frac{Q_2}{Q_1} \cdot N_1 \cdot \frac{D_1^3}{D_2^3} \tag{4.8}$$

By replacing the values for the Lyman extruder ($Q_1 = 0.125Kg/h, N_1 = 13.5rpm, D_1 = 16mm$) and the aimed output flow and starting diameter ($Q_2 = 3kg/h, D_2 = 30mm$), the resulting speed for the screw is:

$$N_2 = 49rpm$$

In a similar way, the needed torque is calculated as follows:

$$T_2 = T_1 \cdot \frac{L_2}{L_1} \cdot \frac{D_2^3}{D_1^3} \tag{4.9}$$

By again replacing the values from the Lyman extruder ($T_1 = 2.942Nm, L_1 = 142mm, D_1 = 16mm$) and from this design ($L_2 = 460mm, D_2 = 30mm$), the obtained torque is:

$$T_2 = 63Nm$$

Thus, it is needed to choose a motor and gearbox that are able to handle a torque of $63Nm$ at the speed of $49rpm$. However, it is important to highlight that these results are estimations, and that the final performance of the extruder may differ, making necessary to do some adjustments in the final prototype.

4.4.3 Nozzle design

In Chapter 3 it is explained that the die geometry, in this case the nozzle, has an influence in the final net flow.

Another important aspect to take into account is that the cross section area has a large influence on the speed that the robot will run at. In order to have a uniform printing, the speed of the robot while printing has to be synchronized with the output flow of the extruder. In other words, the final output flow of the extruder has to be similar to the deposition rate, otherwise the filament will either stretch or accumulate leading to non desirable results. This can be explained with the following equation:

$$Q \approx A \cdot v \tag{4.10}$$

Where Q is the volumetric flow, A is the nozzle channel area and v is the linear speed of the robot while printing. The channel area of the nozzle is:

$$A = \frac{\pi D^2}{4} \tag{4.11}$$

Assuming equality and combining (4.10) and (4.11) gives:

$$v = \frac{4Q}{\pi D^2} \tag{4.12}$$

Thus, for a volumetric flow of $Q = 0.003m^3/h$ ($\approx 3kg/h$), the following table shows the relation between speed and different nozzle diameters:

$D(mm)$	$v(mm/s)$
1	1061
2	265.2
3	117.9
4	66.3
5	42.4
6	29.5
7	21.6
8	16.6

Table 4.1 Relation between nozzle diameter and robot speed for Q=3kg/h.

Furthermore, the cross section area of the die determines the resolution of the printing. A smaller section means higher resolution, but it requires a higher speed and therefore it leads to larger forces when changing directions along the path. This is not desired for the robot and the extruder durability. For this project nozzles of different diameter for air blow guns are used so that they are easily exchangeable for testing purposes. Another design parameter to modify is the speed of the screw, which changes the output flow rate.

4.4.4 Barrel

The barrel design is directly related to the geometry of the screw, and the main requirement is that the inner diameter is adjusted with respect to the screw so that there are as little leakages as possible. The gap should be around 0.001 times the diameter [Rauwendaal, 2001].

In this project, a standard aluminum pipe with an inner diameter of 30mm and an outer diameter of 50mm is used. The choice of the outer diameter is done taking into

account the standard sizes for heater bands and also the overall stiffness. Aluminum is chosen because it is lighter and cheaper than other materials such as stainless steal. A threaded hole is drilled in one of the ends to be able to attach an adaptor for the nozzle. On the other end a pipe of the same diameter made of Teflon is connected. This is done in order to insulate the rest of the extruder, foremost the gearbox and motor, from the heat source.

The Teflon pipe has another threaded hole on the side in order to be able to attach a hopper, as is shown in Figure 4.13.

4.4.5 Motor unit and gearbox

As calculated in Section 4.4.2 the estimated needed torque is $69Nm$, which is significantly high for non industrial stepper and DC motors. For this purpose a stepper motor of model NEMA 42 with the following characteristics is chosen:

Motor type	Bipolar
Step angle	1.8 °
Holding torque	30 Nm
Rated current per phase	8 A
Shaft diameter	19 mm
Weight	12.5 Kg

Table 4.2 Stepper motor specifications.

As Table 4.2 shows, the motor is not capable of delivering the needed torque by itself. Thus a gearbox is needed. A PG080 planetary gearbox from Apex Dynamics with a ratio of 5:1 is used, so that the holding torque would be up to $150Nm$. These are some of the specifications of the gearbox:

Nominal output torque	104 Nm
Emergency stop torque	312 Nm
Nominal input speed	3600 rpm
Efficiency	>97%
Weight	3.5 Kg
Operating temperature	$-10°C \sim 90°C$

Table 4.3 Gearbox specifications.

With the cited specifications, the motor and gearbox should be able to drive the screw according to the calculations, with a certain safety factor.

In order to control the stepper motor, the DM2282 stepper driver is used:

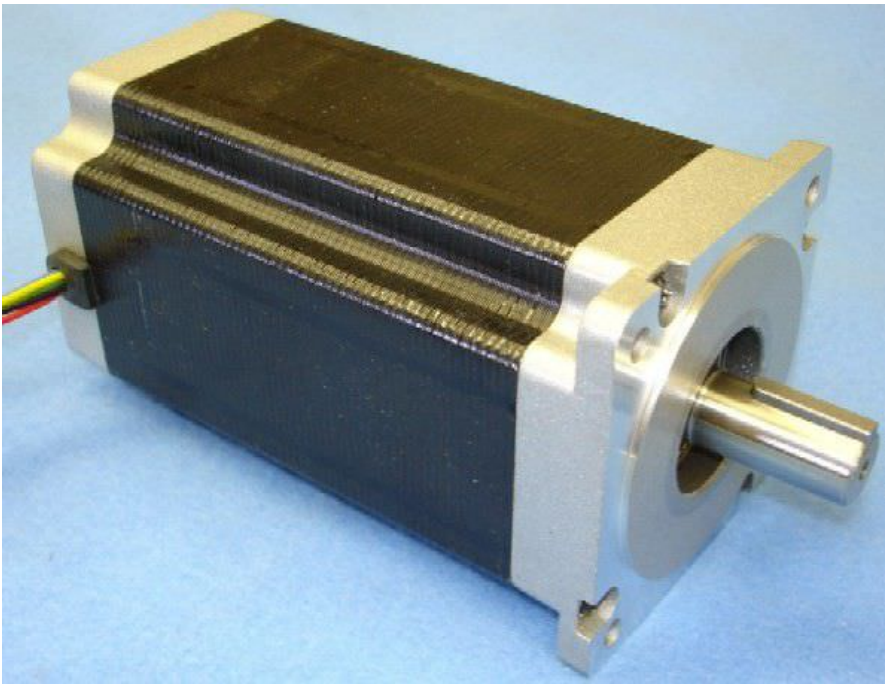

Figure 4.10 NEMA 42 stepper motor.

Maximum output torque	8.2 A
Supply voltage	220V
Maximum pulse frequency	200 kHz
Weight	1.3 Kg
Operating temperature	$-20°C \sim 65°C$

Table 4.4 Driver specifications.

4.4.6 Heater element and controller

A nozzle heater band is used as a heater element since it is a commonly used solution in the industry. The chosen heater is made of stainless steel and has a resistance thread made of Nickel-chrome. It also has a built in J-type thermocouple for temperature feedback. It is rated for $400°C$ and has a power of $600W$.

To control the element an off-the-shelf controller is chosen. The controller uses a PID-control algorithm to control a relay switch that regulates the heater element. Some functionality of the controller is auto tuning of PID parameters and several alarm functions.

Figure 4.11 DM2282 step driver.

Figure 4.12 Heater band and temperature controller.

Both the heater band and the temperature controller are shown in Figure 4.12.

4.4.7 CAD design

Once the primary parts needed are chosen and defined, a 3D CAD model of the extruder is made in SolidWorks. The different previously explained parts are com-

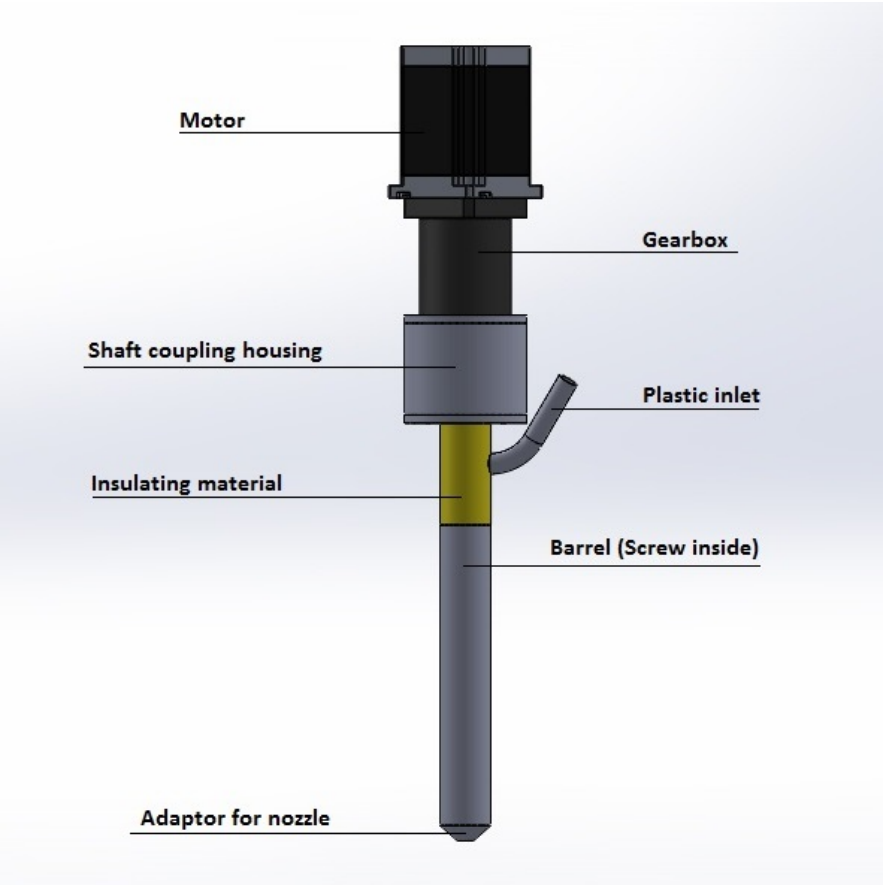

Figure 4.13 Final CAD prototype of the printer head.

bined and other mechanical parts to assembly the extruder are added. In Figure 4.13 the final 3D design of the prototyped extruder is shown.

The other basic parts needed for the extruder are:

- Shaft coupling
- Intermediate adaptor pipe-nozzle
- An intermediate chamber for housing the shaft coupling

In Appendix A 3D views of all parts are available.

4.4.8 Assembly of printer head

The first step to assembly the printer head is to connect the gearbox to the motor. The gearbox is screwed to the motor, and the shaft of the motor is coupled with the gearbox with a known torque of $23Nm$ according to the data sheet. The wire couples to each coil in the stepper motor are then identified and connected to the DM2282 controller. The step resolution is set to 200 steps per revolution (default) and for testing the maximum current is set to $2.2A$. After verifying the assembly the maximum current is successfully increased to $8.2A$. As an input to the controller a function generator is used. The function generator produces a square wave with an amplitude of $5V$ peak to peak. The controller moves the motor one step on falling and rising edge. The speed of the motor and gearbox is then measured with a tachometer to see that it corresponded to the expected frequency of the square wave. This is later used to set the motor to the correct speed.

In order to properly configure the temperature controller, the temperature offset is measured with a pyrometer and then corrected. Then the temperature of the heater element is increased to the working temperature of $230^{\circ}C$ and again measured to calculate the gain of the J-type thermocouple.

5

Results

5.1 Calibration of the L2 robot

The method explained in Section 4.2 is followed obtaining the results shown in Table 5.2. The length of the arms are also measured using the DMM system and the values are presented in Table 5.3. As reference the original parameters are listed in Table 5.1. Notice that the original parameters are expressed in another coordinate frame than the estimated parameters.

Arm	$L(mm)$	$A^0(mm)$	v
1	2054.51	$\begin{bmatrix} 0 \\ 233.73 \\ 1514.6 \end{bmatrix}$	$\begin{bmatrix} 1.0001 \\ -0.00470 \\ -0.00194 \end{bmatrix}$
2	1808.52	$\begin{bmatrix} 0 \\ 1542.55 \\ 1434.02 \end{bmatrix}$	$\begin{bmatrix} 1.0004 \\ -0.0025725 \\ -0.0015314 \end{bmatrix}$
3	1807.83	$\begin{bmatrix} 0 \\ 13.18 \\ 35.65 \end{bmatrix}$	$\begin{bmatrix} 1.0005 \\ -0.00413 \\ 0.00018 \end{bmatrix}$

Table 5.1 The previous parameters used on the L2 robot. It is notable that the absolute value of the direction vectors, $|v|$, is larger than one.

Arm	$L(mm)$	$A^0(mm)$	v
1	2055.92	$\begin{bmatrix} 909.45 \\ -16.32 \\ 1670.01 \end{bmatrix}$	$\begin{bmatrix} 0.99988 \\ -0.0075 \\ 0.01352 \end{bmatrix}$
2	1805.5	$\begin{bmatrix} 883.83 \\ 1293.62 \\ 1624.036 \end{bmatrix}$	$\begin{bmatrix} 0.99988 \\ -0.006566 \\ 0.01363 \end{bmatrix}$
3	1805.87	$\begin{bmatrix} 919.15 \\ -71.3700 \\ 193.98 \end{bmatrix}$	$\begin{bmatrix} 0.999944 \\ -0.005933 \\ 0.008701 \end{bmatrix}$

Table 5.2 The estimated parameters in the measurement frame.

Arm	$L(mm)$
1	2056.16
2	1807.32
3	1806.57

Table 5.3 The measured lengths using the SpaceProbe.

As can be seen, the lengths estimated in the optimization are very similar to the lengths of the arms measured by the SpaceProbe. However the lengths of the arms measured with the SpaceProbe may not describe the kinematics in the right way by themselves, although they serve as a reference to state that the estimated values are meaningful.

5.2 Validation of estimated parameters for L2

5.2.1 Quantitative results

The methodology explained in Subsection 4.3.2 to evaluate the error is followed, taking 48 data points equally spaced as is shown in Figure 5.1.

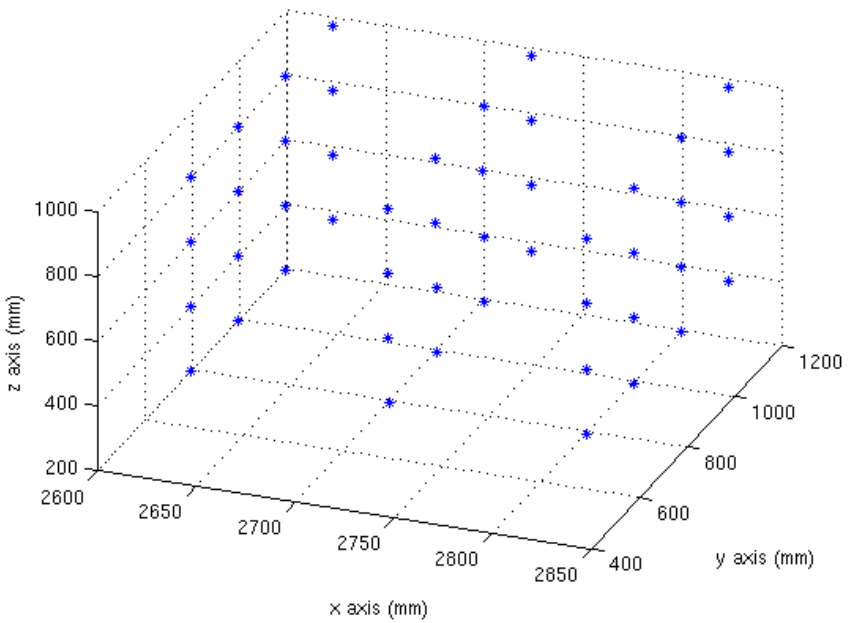

Figure 5.1 Data-point grid in the camera frame.

Then according to Equation 4.6 and Figure 4.7, the absolute error for each point is calculated and is shown in Figure 5.2.

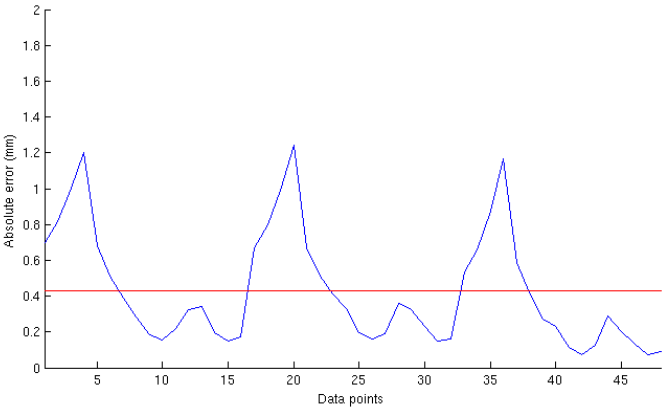

Figure 5.2 Absolute error for each data point.

In Figure 5.3 the individual errors for each axis is plotted.

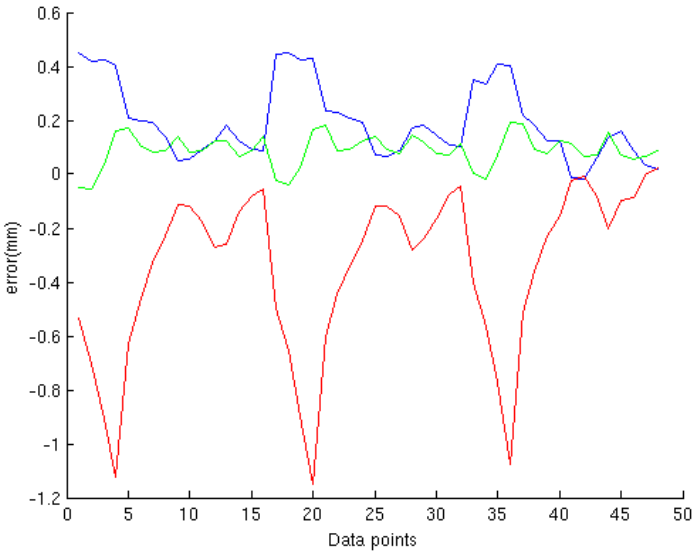

Figure 5.3 Error in X axis (blue), Y axis (red) and Z axis (green) for each data point.

It can be seen that the error follows a pattern in the different Y-Z layers where the error has its maximum in the lower left corner, and minimum in the upper left corner. In Chapter 6, a feasible reason for that is given. However, this error is repeatable which indicates that it might be a systematic error produced by the kinematic model. This systematic error can be compensated when a reference position for the end-effector is given. Thus, the error for each point is saved in a look-up table and used for the compensation, as it is explained in Subsection 4.3.3. The resulting compensating algorithm is tested in 18 other points shown in Figure 5.4. In these points the estimated error is interpolated in the three axes. The resulting absolute error is shown in Figure 5.5.

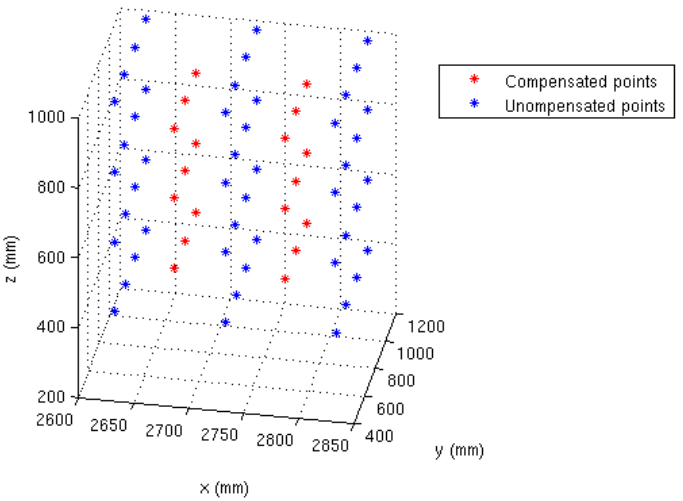

Figure 5.4 Data-point grid with compensated and uncompensated points.

As can be seen in Figure 5.5, the peak error is reduced, and also the mean error. However, as elaborated on in Chapter 6, the result is not as satisfactory as expected.

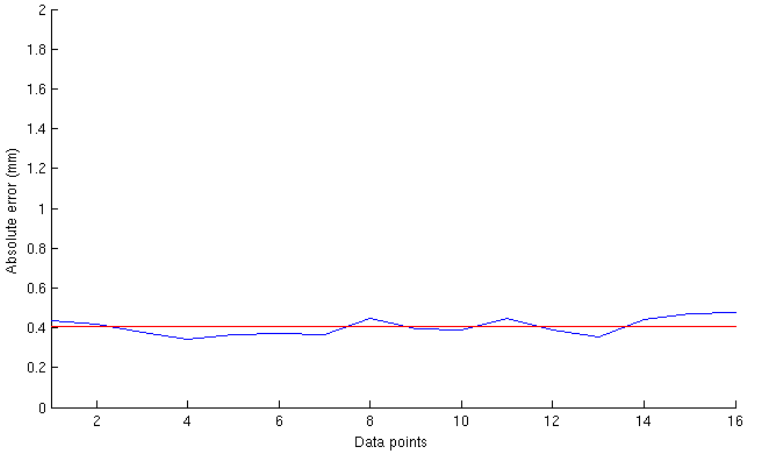

Figure 5.5 Absolute error after compensation for each data point.

5.2.2 Qualitative results

The results from the circle experiment explained in Section 4.3.1 is presented below. The parameters refereed to as new are the ones acquired through the optimization method described in Section 4.2 and shown in Table 5.2. In Figure 5.6 the different locations in the workspace of the measured circles are shown.

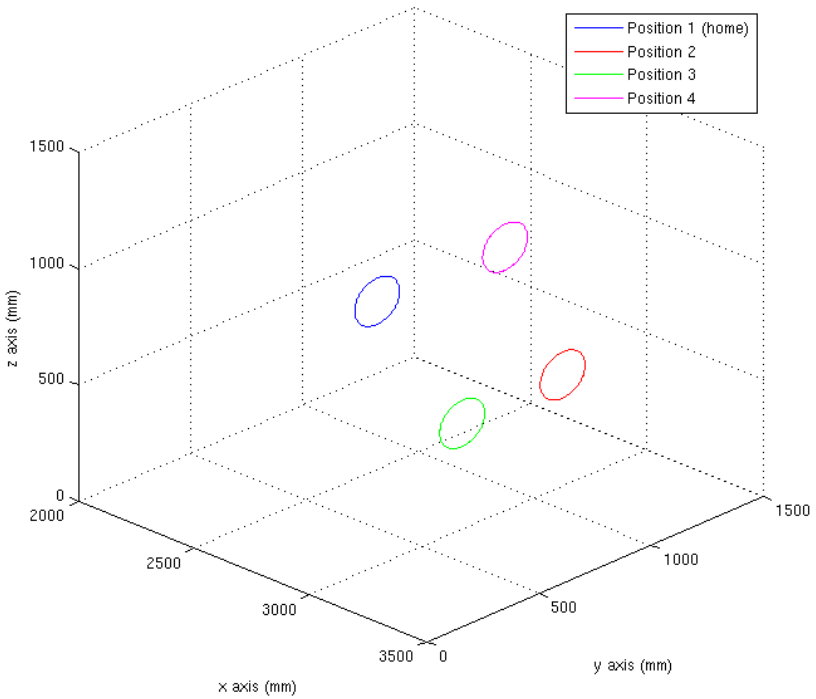

Figure 5.6 A figure showing where the circles are made in the workspace.

In Figure 5.7 the result of the least-squares method for finding the plane that contains the circle is shown . This is shown for two different sets of parameters, the one estimated in the optimization (red), and another set of parameters that is chosen arbitrarily (blue), to give an inaccurate kinematics model. This is used to see with the naked eye how much it affects the shape of the circle. The green rectangles show the optimized planes that contain the circles.

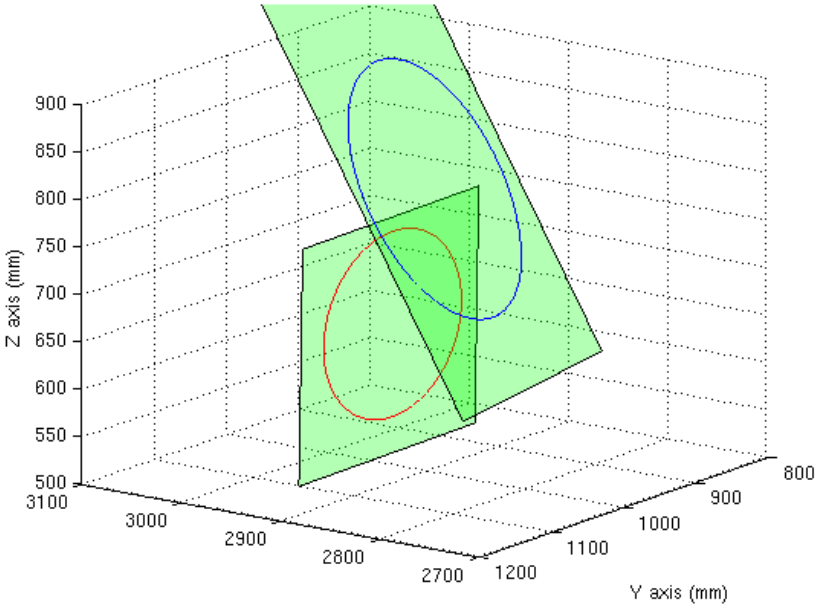

Figure 5.7 In red a circle with the optimized parameters and in blue a circle with arbitrarily chosen parameters.

In Figure 5.8 the error for the first circle of Figure 5.6 is shown. The other circles have similar errors and their results are omitted. The mean error for the original parameters are 1.865*mm* and for the new optimized parameters the mean error is 0.046*mm*.

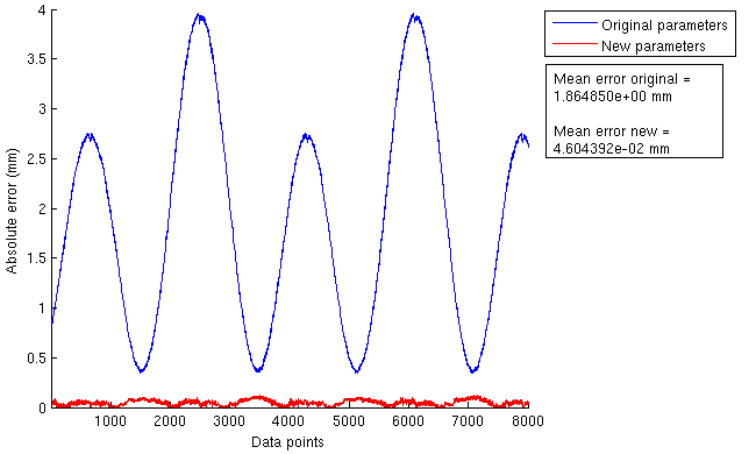

Figure 5.8 The error for the first circle with both old and new parameters.

5.3 Printer head prototype

Below the assembled 3D printer head prototype is shown in Figure 5.9.

Figure 5.9 The 3D printer head prototype mounted on the L2 robot in the Robot Lab at LTH.

6

Conclusions

6.1 Calibration of the L2

As shown in Subsection 5.2.1, Figure 5.2, the absolute accuracy of the robot after the calibration and without any compensation has a mean value over 0.4*mm* with some peaks reaching 1.2*mm*, when the end-effector is close to the limits of the workspace. This is due to the fact that the sensitivity of the end-effector position with respect to the joint position is not constant along the rails. This sensitivity increases as the angle between the arm and the rail becomes bigger, and thus, the same error for the joint position will lead to magnified errors in the final position of the end-effector [Dressler, 2012].

However as explained in Subsection 4.3.3, it is found that there is a systematic error that could be compensated for since it is repeatable along the different points where the validation is performed. After the compensation, successful results are obtained, decreasing the peak error from 1.2mm to 0.5mm, and also decreasing the mean error. Nevertheless, the results of the compensation are not as satisfactory as expected. A feasible reason for this is that the camera might have been moved slightly before the compensation so that the results are distorted. It is known that the place where the camera is located is subjected to vibrations and also there is a risk that people move the camera accidentally. This is implied by redoing the validation process in the same points without compensation and realizing that the error is in overall doubled. The hypothesis is that because the camera might have been moved slightly out of position, the gathered data is not representative, and the actual difference between reference position and real position is less than the one showed in Figure 5.5.

In order to prevent the data to be corrupted due to a camera movement, a dynamic frame is tried out. The dynamic frame is made of 3 LEDs whose relative position between them is constant. The dynamic frame is then attached via software to the reference frame defined with the SpaceProbe, so that if the camera is moved, it is still able to know the position of other LEDs with respect to the reference frame, as long as the dynamic frame is visible. Nevertheless, this method is not successful

since the noise level is increased up to 2*mm*, which is unacceptable for this purpose. The sources or reasons for this noise are unknown.

In Subsection 5.2.2, a qualitative comparison between the old kinematic parameters and the new parameters estimated during this project is shown. It is noticeable how the robot is more capable of following a given path with a smaller error, in this case a circle. For the old kinematic parameters, the error is reaching 4*mm* at some points, whereas for the new optimized parameters, the maximum error is only about 0.1*mm*. It is important to highlight that this error is not the absolute accuracy. It rather measures how similar is the followed path to a circle without taking into account systematic errors in the model and that is the reason why this error is considerably lower than the absolute accuracy.

A quantitative comparison between the old and the new optimized parameters cannot be shown since they are referred to different frames, and it is not possible to define a frame perfectly equal to the one where the old values are defined. However, it is clear with the qualitative experiment that the overall accuracy and performance of the robot is significantly improved. This might be due to the fact that the old kinematic parameters had some faulty terms, like the direction vectors of the rails. As shown in Table 5.1 the direction vector length is larger than 1 when it should actually be equal to 1.

To minimize all sources of errors from the camera and in general to improve the performance of the robot, the following considerations should be taken into account. The camera is not temperature calibrated, so the values could be biased by some micrometers. Regarding this, a camera calibration would increase the accuracy of the camera even more, although the final result would probably not differ in a measurable amount since the error is in the range of hundreds of micrometers. Another improvement would be achieved by performing the calibration in discrete points instead of in a continuous path, since the result would not be affected by the dynamics of the robot, nor the performance of the control system. It is also recommended to have an even distribution of the points along the workspace so that the optimization weights the error in the same amount for every point in the space. All the process should be carried out in the shortest possible time to prevent the camera to be accidentally moved during the calibration process.

6.2 Printer head

As already mentioned in Section 2.2, the goal of designing a printer head was added late in the project and thus, it was not possible to completely finish the prototype due to time constraints. As a general method to calibrate a Gantry-Tau robot has been developed, and a printer head for large scale printing has been prototyped, this should serve as an interesting starting point for a continued project. This is further discussed in Chapter 7, Future work.

7

Future work

This project serves as a starting point for a wider project where the purpose is to print larger objects in less time and with more quality by using the advantages of a parallel kinematic robot and the output capacity of larger printer heads. As explained in Section 2.2, there are some goals that could not be achieved due to time constraints. It has also been explained through out the project that certain procedures could have been improved. Some of the things that could be studied and developed in following projects are listed and explained below:

- **Measure the orientation:** More LEDs could be placed on the end-effector to measure the orientation which could be useful to know.
- **Calibrating the F1 robot:** Calibration was not performed, so future projects could follow the procedures explained in this project to perform the calibration. The F1 robot has a higher maximum workload, and thus, it could handle even larger printer heads. It also has a larger workspace that allows for bigger printed objects. The vertical orientation of the F1 workspace is also an advantage.
- **Using more degrees of freedom:** The available 3D printers in the market use 3 degrees of freedom for printing. This leads to a staircase effect that may decrease the quality of the product. This effect is more noticeable when the resolution is lower, since the thickness of each layer is higher. However this could be solved by making use of the advantages of a robot like the L2 or the F1 with 5 or 6 DOF. This would allow to print in non conventional paths, i.e., not layer by layer. Nevertheless, available slicing software for 3D printing does not support this option, and thus this would require new software or modifications to existing ones.
- **Automatic synchronization of robot and printer head:** As it is explained in Subsection 4.4.3, the speed of the robot has to be synchronized with the output flow of the printer head. ABB has developed a system that outputs a frequency pulse signal for the control of a motor depending on the linear

speed of the robot. This could be used to do this synchronization automatically.

- **Developing a low-cost temperature controller:** Due to the fact that it was decided to build the extruder at the end of the project, there was no time to solve this control problem. In a future project this could be done with the help of e.g., an Arduino board.

- **Improving the printer head:** The design of the extruder could be optimized by performing a finite element analysis, since it would be possible to simulate the heat flow and also the strain in the extruder. From the results some design decisions might be taken, such as adding more heaters to have a more linear profile of temperatures in the extruder. Also a proper extrusion screw might be used instead of a drill bit, since a proper extrusion screw has an optimized geometry for this function, and hence increasing the final output flow and decreasing the needed torque.

- **Printing with other materials:** There exist some other projects that are aiming to print with other materials such as concrete or chocolate, which could be combined with the advantages of a parallel kinematic robot. Examples of what could be printed are concrete furniture for public places such as benches, or large chocolate sculptures [Deyle, 2013][Serra Gómez, 2015].

Bibliography

A. W. Birley, B. H. and J. Batchelor (1992). *Physics of Plastics: Processing, Properties and Materials Engineering*. ISBN 3-446-16274-7. Hanser Publishers, Munich, Germany.

Blomdell, A., I. Dressler, K. Nilsson, and A. Robertsson (2010). "Flexible application development and high-performance motion control based on external sensing and reconfiguration of ABB industrial robot controllers". In: *2010 IEEE International Conference on Robotics and Automation*, pp. 62–66.

Coope, I. (2000). "Reliable computation of the points of intersection of n spheres in r^n". *ANZIAM Journal* **42**, pp. C461–C477.

Deyle, T. (2013). *Large-scale rapid prototyping robots: industrial robot arm extruders and building-scale 3d printers*. `http://www.hizook.com/blog/2013/11/13/large-scale-rapid-prototyping-robots-industrial-robot-arm-extruders-and-building-sca`.

Dressler, I. (2012). *Modeling and Control of Stiff Robots for Flexible Manufacturing*. PhD thesis ISRN LUTFD2/TFRT--1093--SE. Department of Automatic Control, Lund University, Lund, Sweden.

Excell, J. and S. Nathan (2010). *The rise of additive manufacturing*. `http://www.theengineer.co.uk/in-depth/the-big-story/the-rise-of-additive-manufacturing/1002560.article`. Last checked: 04.06.2015.

Fab@Home Project (2015). `http://www.fabathome.org/`. Last checked: 28.01.2015.

H. F. Giles, J. R. W. and E. M. Mount (2005). *Extrusion, The Definitive Processing Guide and Handbook*. ISBN: 978-0-8155-1473-2. William Andrew, Norwich, New York, USA, pp. 13–34.

Halterman, T. (2013). *Dirk van der Kooij 3d prints endless chair with robotic arm*. `http://www.3dprinterworld.com/article/dirk-van-der-kooij-3d-prints-endless-chair-with-robotic-arm-and-recycled-refrigerators`. Last checked: 04.06.2015.

K-Series Optical CMM solutions (2010). https://www.nikonmetrology.com/content/download/11040/220148/version/4/file/Optical_CMM_EN.pdf.

Lyman, H. (2012). *Lyman filament extruder*. http://www.thingiverse.com/thing:34653. Last checked: 04.06.2015.

Manias, E. (2012). *Flows in polymer processing*. http://zeus.plmsc.psu.edu/~manias/MatSE447/. Last checked: 04.06.2015.

Medeni Maskan, A. A. (2011). *Advances in Food Extrusion Technology*. ISBN 9781439815205. CRC Press, Boca Raton, Florida, USA.

MONROE (2015). *MONROE - Hyper-modular open networked robot systems with excellent performance*. http://echord.info/wikis/website/monroe. Last checked: 12.06.2015.

NASA (2014). *Space station 3-d printer builds ratchet wrench to complete first phase of operations*. http://www.nasa.gov/mission_pages/station/research/news/3Dratchet_wrench. Last checked: 29.05.2015.

Rauwendaal, C. (2001). *Polymer Extrusion*. ISBN US: 1-56990-321-2. Hanser Publishers, Munich, Germany.

RepRap Project (2015). http://reprap.org/. Last checked: 28.01.2015.

Robertz, S. G., L. Halt, S. Kelkar, K. Nilsson, A. Robertsson, D. Schär, and J. Schiffer (2010). "Precise robot motions using dual motor control". In: *2010 IEEE International Conference on Robotics and Automation, May 3-8*. Anchorage, Alaska, pp. 5613–5620.

Serra Gómez, B. (2015). *Construction and software design of an ABB IRB 140 concrete 3D printer*. Tech. rep. Department of Product Development, Lund University, Sweden.

SMErobot (2015). *SMErobot^{TM} - the European robot initiative for strengthening the competitiveness of SMEs in manufacturing*. http://www.smerobot.org/. Last checked: 12.06.2015.

SolidsWiki. Extrusion Screws. http://solidswiki.com/index.php?title=Extrusion_Screws. Last checked: 04.06.2015.

Tyapin, I., G. Hovland, and T. Brogårdh (2007). "Workspace optimisation of a reconfigurable parallel kinematic manipulator". In: *Advanced intelligent mechatronics, 2007 IEEE/ASME international conference on, September 4-7*. Zurich, pp. 1–6. DOI: 10.1109/AIM.2007.4412413.

Wikipedia. Plastic extrusion. http://en.wikipedia.org/wiki/Plastics_extrusion. Last checked: 04.06.2015.

Wikipedia. Triangulering. http://sv.wikipedia.org/wiki/Triangulering. Last checked: 04.06.2015.

Wohlers Associates (2014). http://www.wohlersassociates.com/press65.html. Last checked: 04.06.2015.

Zhang, G. Q., X. Li, R. Boca, J. Newkirk, B. Zhang, T. A. Fuhlbrigge, H. K. Feng, and N. J. Hunt (2014). "Use of industrial robots in additive manufacturing - a survey and feasibility study," in: *ISR/Robotik 2014; 41st International Symposium on Robotics; Proceedings of, February 6 - March 6*. Munich, Germany, pp. 1–6.

A

Printer head drawings

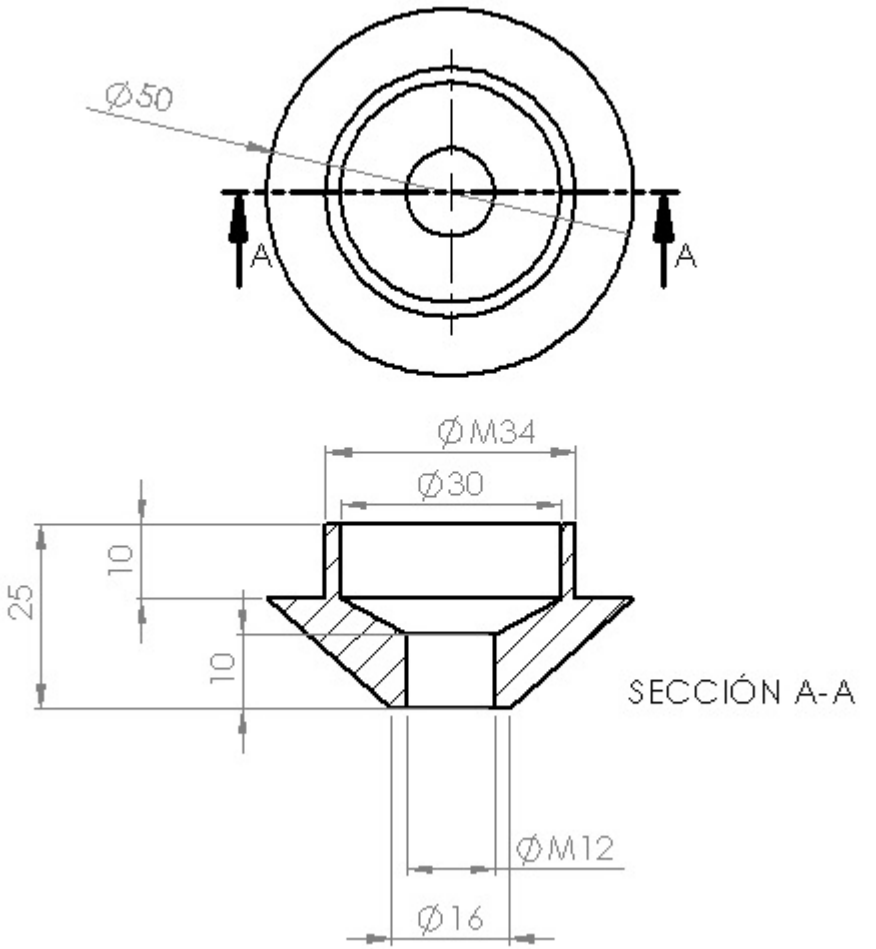

Figure A.1 Nozzle-barrel adaptor.

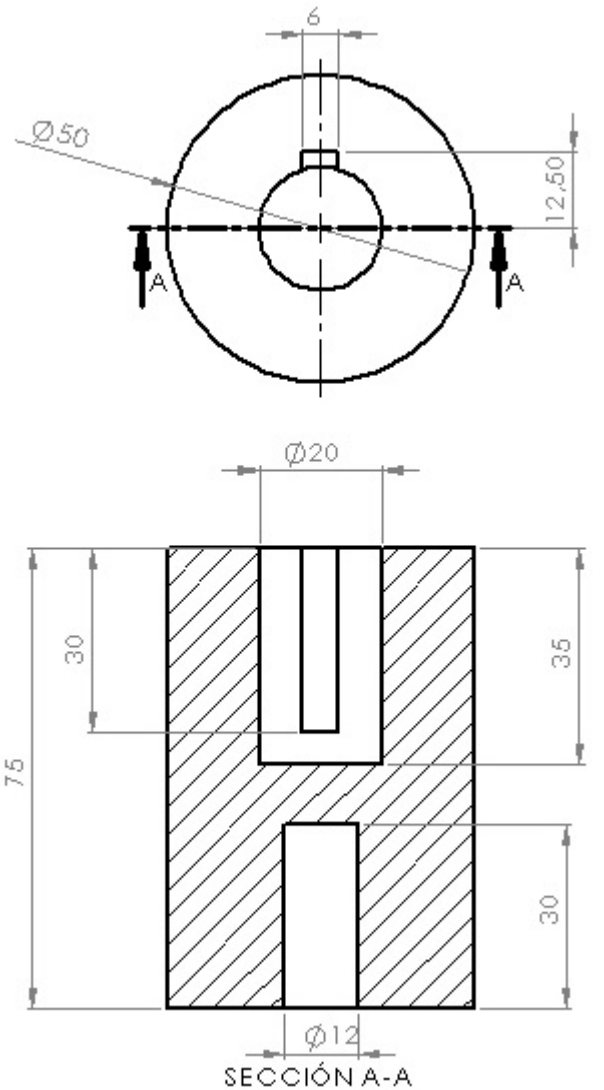

Figure A.2 Shaft coupling.

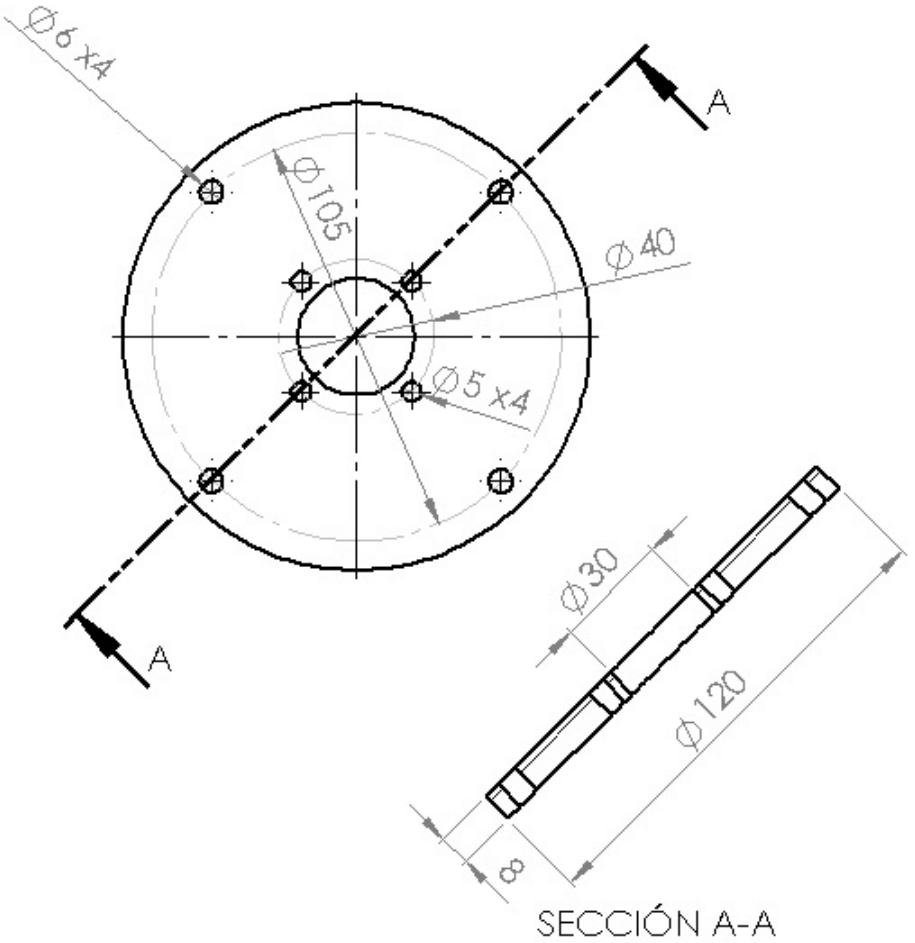

Figure A.3 Chamber-barrel adaptor.

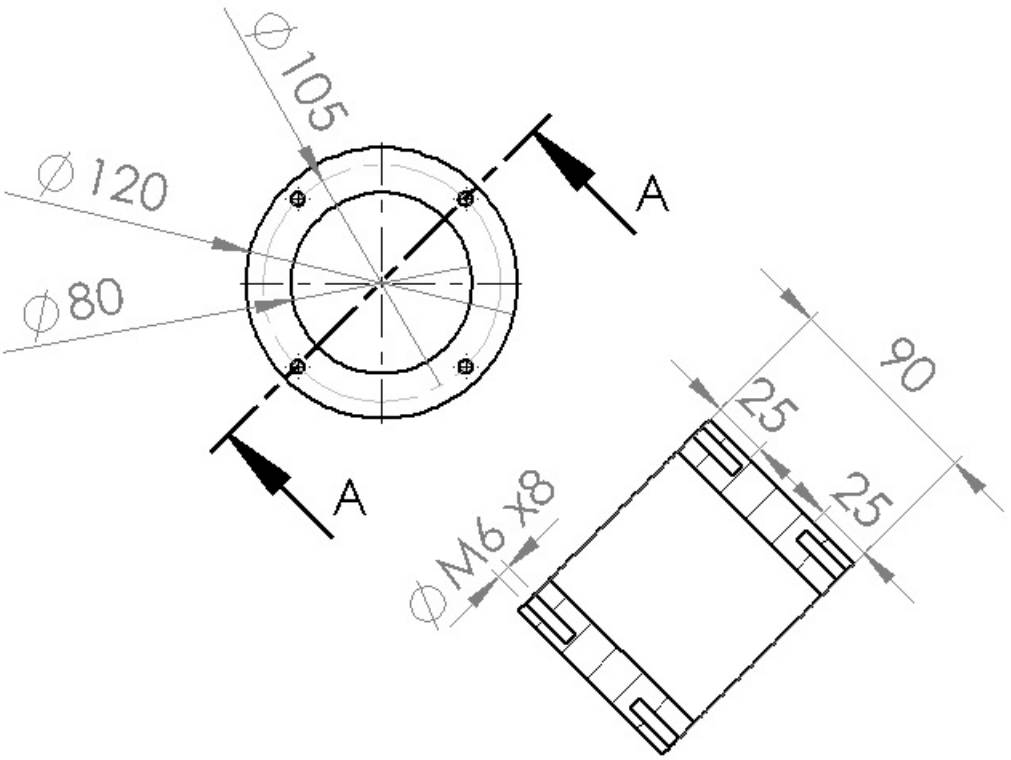

Figure A.4 Shaft coupling housing.

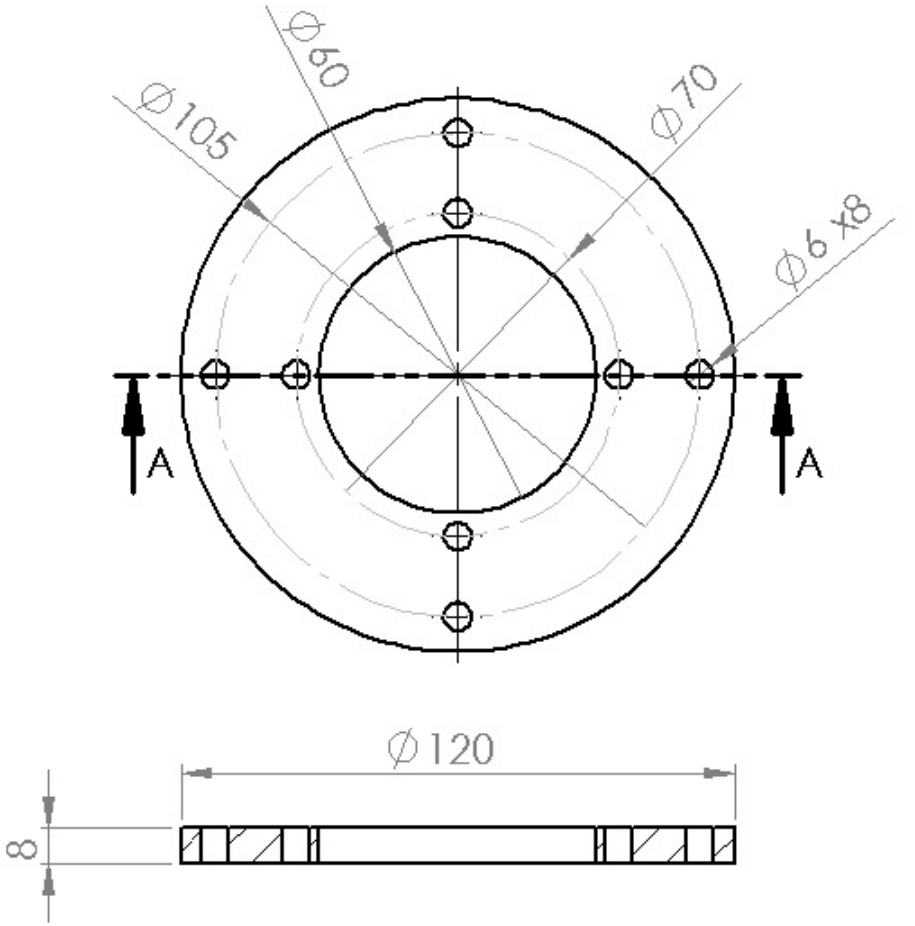

Figure A.5 Gearbox-chamber adaptor

Lund University
Department of Automatic Control
Box 118
SE-221 00 Lund Sweden

Document name
MASTER´S THESIS

Date of issue
June 2015

Document Number
ISRN LUTFD2/TFRT--5978--SE

Author(s)
Patrik Lilja
Jorge Sola Merino

Supervisor
Anders Robertsson, Dept. of Automatic Control, Lund University, Sweden
Rolf Johansson, Dept. of Automatic Control, Lund University, Sweden (examiner)

Sponsoring organization

Title and subtitle

Calibration of Gantry-Tau Robot and Prototyping of Extruder for 3D Printing

Abstract

This master thesis is about improving the accuracy of a Gantry-Tau robot by identifying the key parameters in the kinematics of the robot. This is done using a vision system and then estimating the parameters by minimizing the closure equation of the kinematics. The robot with improved control is then used for additive manufacturing. Furthermore, a prototype for a large plastic printer head is presented.

Keywords

Classification system and/or index terms (if any)

Supplementary bibliographical information

ISSN and key title
0280-5316

ISBN

Language
English

Number of pages
1-62

Recipient's notes

Security classification